SCIENCE SUPPORT FOR SPACE-BASED DROPLET COMBUSTION: DROP TOWER EXPERIMENTS AND DETAILED NUMERICAL MODELING[+]

Anthony J. Marchese[*] and FREDERICK L. DRYER
Department of Mechanical and Aerospace Engineering
Princeton University, Princeton, NJ 08544
fldryer@phoenix.princeton.edu

Introduction

This program supports the engineering design, data analysis, and data interpretation requirements for the study of initially single component, spherically symmetric, isolated droplet combustion studies. Experimental emphasis is on the study of simple alcohols (methanol, ethanol) and alkanes (n-heptane, n-decane) as fuels with time dependent measurements of drop size, flame-stand-off, liquid-phase composition, and finally, extinction. Experiments have included bench-scale studies at Princeton, studies in the 2.2 and 5.18 drop towers at NASA-LeRC, and both the Fiber Supported Droplet Combustion (FSDC-1, FSDC-2) and the free Droplet Combustion Experiment (DCE) studies aboard the shuttle.

Test matrix and data interpretation are performed through spherically-symmetric, time-dependent numerical computations which embody detailed submodels for physical and chemical processes. The computed burning rate, flame stand-off, and extinction diameter are compared with the respective measurements for each individual experiment. In particular, the data from FSDC-1 and subsequent space-based experiments provide the opportunity to compare all three types of data simultaneously with the computed parameters. Recent numerical efforts are extending the computational tools to consider time dependent, axisymmetric 2-dimensional reactive flow situations. The sections below summarize recent progress.

Detailed Kinetic Modeling Of N-Alkane Droplet Combustion [1]

There is a critical need for partially-reduced, high temperature, n-alkane kinetic mechanisms which accurately reproduce a wide variety of kinetic and flame observations, which are sufficiently small for use in transient, uni-dimensional reactive flow computations, and which can serve as skeletal models for developing even smaller reduced representations for multi-dimensional, time-dependent computations and rate-ratio asymptotic studies. Such a mechanism has been developed for n-heptane [2], and the technique utilized can easily be extended to consider larger alkanes and mixtures. The mechanism considers fuel thermal decomposition reactions and realistically accounts for the site-specific abstraction of hydrogen atoms and the subsequent heptyl radical β-scission processes. Validation against kinetic data from stirred reactors, a flow reactor, shock tubes, and laminar flames were first performed. The mechanism was then incorporated in transient, spherically symmetric, isolated droplet calculations using a time-dependent, finite element, chemically reacting flow model [1,3] which also considers detailed molecular transport [4]. No kinetic or gas-phase transport parameters were modified to achieve agreement with experimental results. The only free parameter in the model is that utilized to approximate enhanced mass transfer due to internal liquid-phase motion [5]. Internal motions are inherent in experimental droplet deployment techniques and may also result from thermal and/or solutal Marangoni effects, but not from gas-phase convective motions relative to the droplet[5]. The development was motivated primarily by DCE experiments[6], first flown aboard Space Shuttle Columbia (STS-83) in April, 1997

The entire combustion history (ignition, premixed/diffusive flame transition, droplet heating, vapor accumulation, quasi-steady combustion, and extinction/burn out) were calculated. Ignition delay experiments [7] were simulated and, during quasi-steady combustion, the calculated droplet flame structures were compared with calculations using an earlier mechanism proposed by Warnatz [8]. For the combustion of small (< 1 mm) heptane droplets in air at 1 atm,

Paper Presented at the **Fourth International Microgravity Combustion Conference**, Clevleland, Ohio, May 19-21, 1997
Work funded under NASA Grant No. NAG3-1231 and COOP No. NCC3-487

[*]Current address: School of Engineering, Rowan College, Glassboro, NJ 08028, *marchese@rowan.edu*

[+]Visit our Web Site at *http://www.princeton.edu/~fldryer/nasa.dir/*

the model predicts very small extinction diameters which is consistent with the results of Hara and Kumagai [9] and Yang and Avedisian [10] who observed either "burn-out" (i.e. extinction diameter too small to measure) or extinction diameters of less than 100 microns.

The DCE experiments consider large (1 - 5 mm), single component (n-heptane) droplets burned in He/O_2 oxidizing environments of various O_2 content at atmospheric and sub-atmospheric pressures. Reduced pressures and inert substitution reduce sooting propensity and increase extinction diameters [11,12], thus enabling accurate experimental measurements which are not perturbed by sooting effects.

Figure 1 compares the species and temperature calculated using the new mechanism and the semi-empirical mechanism of Warnatz and reveals a dramatic difference in the C_2 and C_3 intermediate distributions. In terms of maximum mass fraction, the new mechanism predicts an increase in C_2H_4 and C_2H_2 production by factors of 8 and 3, respectively, and a 4-fold decrease in maximum C_3H_6 mass fraction. However, both mechanisms predict a similar flame position (location of maximum flame temperature) and similar distributions of major species (O_2, CO, CO_2).

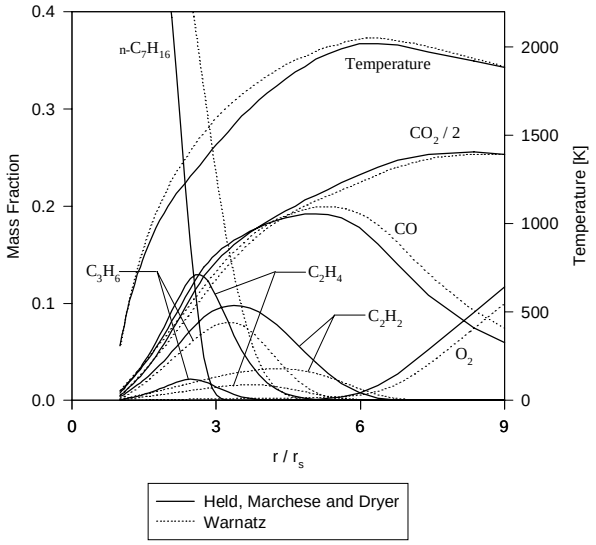

Figure 1. Calculated temperature and gas phase species C_7H_{16}, O_2, C_2H_4, C_2H_2, C_3H_6, and CO for the combustion of an n-heptane droplet at 1.0 second after ignition in an oxidizing environment of 40% O_2 / 60% He at 0.25 atm.

The latter result is consistent with the diffusion flame modeling study of Bui-Pham and Seshadri [13] where temperature and major species measurements were reasonably reproduced using the Warnatz mechanism. For the intermediate C_2 and C_3 species, the new mechanism also appears to be in better qualitative agreement with the experimental measurements of Hamins and Seshadri [14]. There, the measured ordering of these compounds was $C_2H_4 > C_2H_2 > C_3H_6$. At the conditions of Fig. 1, the reaction responsible for the largest percentage of fuel consumption (23.96%) was thermal decomposition:

$$C_7H_{16} \rightarrow C_2H_5 + 1 - C_5H_{11}.$$

The second-leading consumption reaction (17.36%) was the H-atom abstraction via H radical attack leading to 2-heptyl:

$$C_7H_{16} + H \rightarrow 2 - C_7H_{16} + H_2.$$

In overall terms, fuel thermal decomposition accounted for 50.2% of all the fuel consumption, while all of the fuel + H radical attack reactions accounted for an additional 46.6%. The only other class of reactions responsible for greater than 1% of the overall fuel consumption were the fuel + CH_3 radical attack reactions. These observations are important to further reduction of the mechanism and emphasize the significance of decomposition in large-hydrocarbon diffusion flames.

OH* Chemiluminescence Imaging Of Microgravity Droplet Flames [15]

In hydrocarbon flames, the following reaction is known to be a principal source of electronically-excited hydroxyl radicals, OH* [16]:

$$CH(^2\Pi_u) + O_2(^3\Sigma_g) \xrightarrow{k_1} CO(^1\Sigma^+) + OH^*(^2\Sigma^+).$$

The OH* radicals are consumed through the competing reactions:

$$OH^*(^2\Sigma^+) + M \xrightarrow{k_2} OH(^2\Pi) + M$$

$$OH^*(^2\Sigma^+) \xrightarrow{k_3} OH(^2\Pi) + h\nu$$

where the former reactions correspond to quenching by various collisional partners, M, and the last reaction corresponds to the electronic transition $^2\Sigma^+ - ^2\Pi$ which is observed as an ultraviolet OH emission band at 306.4 nm.

Chemiluminescence measurements, along with detailed predictions of electronically-excited hydroxyl radical concentration, have been demonstrated as a means of quantitatively comparing experimental and computed flame position and structure [15]. The procedure is applied in DCE, where an intensified array video camera is used to measure OH* chemiluminescence within the droplet diffusion flame [6]. To develop and validate the approach, isolated microgravity droplet combustion experiments were conducted in drop towers using n-heptane and methanol fuels. Hydroxyl chemiluminescence chemistry was incorporated into a detailed droplet combustion model, thus yielding

OH* as one of the predicted parameters. The chemiluminescence mechanism is discussed elsewhere [1].

Tests were conducted using similar, but separate experimental rigs in the 2.2 second and 5.18 second Zero Gravity Facility (ZGF) drop towers at NASA-LeRC. The generic design of the rigs is described in detail elsewhere [1]. A high speed motion picture camera recorded black and white, back-lit droplet images at 200 frames per second. The OH* radical chemiluminescence images were acquired using a Xybion ISG-250 intensified-array CCD video camera fitted with a 50 mm, UV lens and narrow band interference filter centered at 310 nm (full-width, half-maximum of 10 nm). The Xybion video (and high-speed camera) images were analyzed using a PC-based image analysis system.

To reconstruct the desired OH* emission-intensity distribution, F(r), given the measured line-of-site projection, P(r), the inverse Abel transform was performed:

$$F(r) = -\frac{1}{\pi}\int_r^\infty \frac{P'(\rho)}{(\rho^2 - r^2)^{1/2}}\, d\rho$$

where P'(r) is the derivative of P with respect to radius, r. A least-squares smoothing algorithm was first applied to the data, followed by the three-point Abel deconvolution algorithm.

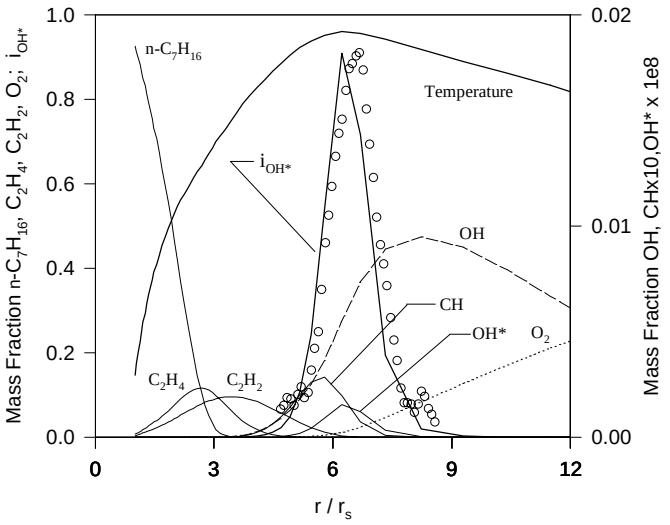

Figure 2. Comparison of computed mass fractions of species v. radial position, with the normalized experimental OH* distribution at 1 second after ignition. Fuel: n-heptane; Initial diameter: 1.9 mm; Environment: 40% O_2/60% He, 0.25 Atm.

The numerical model predicts the peak CH mass fraction to be very near the radius of maximum flame temperature, where the O_2 mass fraction also approaches zero (Fig. 2). Thus, in accordance with the $CH + O_2 \rightarrow CO + OH^*$ route of OH* production, the model predicts the peak OH* mass fraction (and, consequently the peak OH* emission) to occur at a slightly greater radius than that of the maximum flame temperature. Note that the OH* and CH profiles within the flame are very narrow and better define flame features that the temperature profile, which is much less well defined in terms of peak shape.

The data analysis procedure outlined above was also applied to methanol droplet combustion, with similar modifications of an earlier developed numerical model [5**,** 15]. Methanol combustion produces very little CH radical, and examination of the reaction fluxes showed that the $CH+O_2$ reaction was not responsible for the production of OH*. Rather, OH* was produced (in the minute quantities necessary) through thermal excitation processes.

Drop Tower Experiments: Methanol / Water Mixtures

In order to further experimentally validate the droplet combustion model for methanol, calculations were compared with initially pure methanol and methanol/water mixture droplet combustion experiments conducted in the 2.2 second drop tower facility at NASA-LeRC [17]. Tests were performed in oxidizing environments of 18%-35%O_2/N_2 with initial liquid water contents of 0-20%. Instantaneous droplet diameter measurements were made using back-lit, high-speed photography, along with instantaneous flame position determined by monitoring chemiluminescence of electronically-excited hydroxyl radicals (OH*), as described above. Burning rates and flame stand-off ratio time histories for a wide array of methanol and methanol/water droplet combustion conditions were compared with the model results.

In Fig. 3, the experimental data have been five-point averaged and both axes have been normalized by the initial diameter-squared since initial diameter of the droplets varied between 1000 and 1500 mm. The measured burning rate increases substantially with increasing oxygen content and agreement between measured and calculated diameter history is excellent.

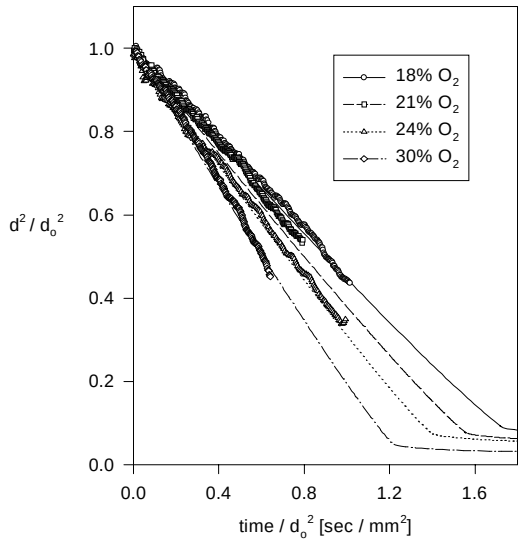

Figure 3. Experimental and numerically predicted data for initially pure methanol droplets burning in various nitrogen/oxygen environments at 1 atmosphere.

The flame position (Fig. 4) was measured using the OH* chemiluminescence method as described in the previous section. In methanol droplet combustion, the flame position is expected to decrease with time once the droplet begins to re-vaporize water which is absorbed into the liquid phase earlier in the combustion process. The increased water within the flame zone decreases the flame temperature, which in turn causes the flame to move closer to the surface. In the experiments, the burn times were not sufficient to observe regasification of condensed water. Thus, after the initial transient period, the flame position was very nearly constant for each initial oxygen content.

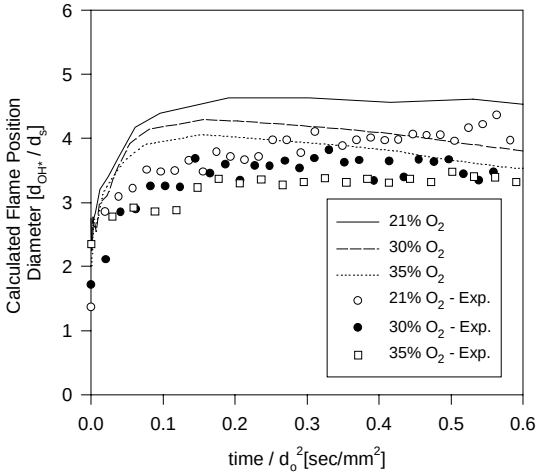

Figure 4. Measured and predicted instantaneous flame position, d_f/d_S, for methanol droplets in 21%, 30%, and 35% O_2 with N_2 inert at 1 atm. pressure.

As expected, the flame position decreased with increasing oxygen content due to stoichiometry considerations. After an initial transient period, average normalized flame positions of 4.1, 3.6, and 3.4 were measured for oxygen contents of 21%, 30% and 35%, respectively. Thus in addition to accurately predicting the burning rate, the model simultaneously predicts the flame position to within one normalized diameter at each condition.

Thermal Radiation Effects: FSDC-1 Results

In October 1995, the first ever space-based droplet combustion experiments, FSDC-1, were conducted aboard the Second United States Microgravity Laboratory (USML-2) mission, on Space Shuttle Columbia. Preliminary results for these experiments, which included methanol, methanol/water mixtures, heptane and heptane/ hexadecane mixtures as fuels, have been summarized earlier [18]. More recently, further numerical modeling for methanol and methanol/water experiments confirms that radiative effects are significant in experiments with initial diameters greater than 1 mm [19, 20]. For the first time, computed burning rate, flame stand-off, and extinction diameter are simultaneously compared with experiments.

To model the effect of non-luminous, radiative heat loss from the droplet flame, the gas phase conservation of energy was modified to include the radiative heat flux, q_R [1,19]. By considering the droplet and infinity as concentric spheres separated by a radiating medium, the formulation of Viskanta and Merriam [21,22] was used to calculate the divergence of the net radiative flux:

$$\nabla \cdot q_R = \frac{1}{r^2}\frac{\partial}{\partial r}(r^2 q_R) = \kappa_P \left[4\sigma_B T_g^4 - G(r)\right].$$

The Planck-mean absorption coefficient, k_P, was calculated locally in space and time, from the calculated gas phase temperature and mole fractions of CO, CO_2, and H_2O. To describe the variation in Planck-mean absorption coefficient with temperature for each of these species, polynomials were fitted to the curves presented in Tien [23].

Figures 5 and 6 are plots of diameter-squared and instantaneous burning rate, respectively, vs. time for 5 millimeter initial diameter methanol/water droplets.

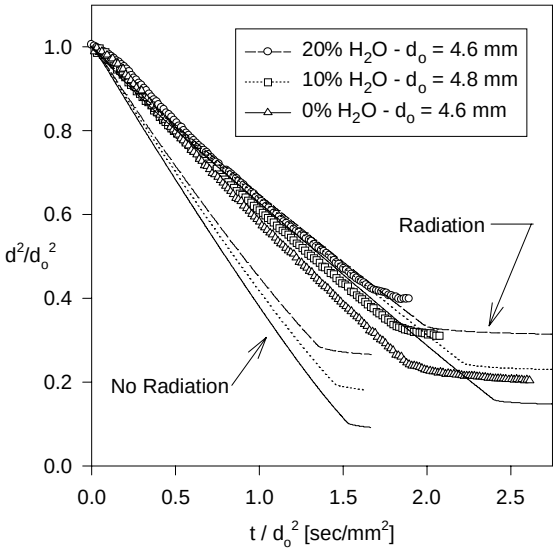

Figure 5. Measured and calculated diameter squared for 5 mm methanol/water droplets.

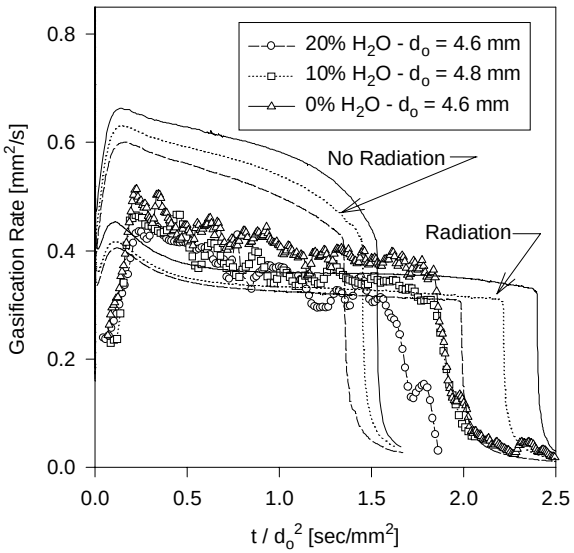

Figure 6. Measured and calculated instantaneous burning rate for 5 mm methanol/water droplets.

The results show that the extinction diameter increases and the burning rate decreases with increasing initial water content. The results also show that at initial droplet diameters of this size, the effect of radiation can no longer be ignored. In the calculations in which radiation is neglected, the numerical model greatly over-predicts the burning rate and under-predicts the extinction diameter. In the calculations that include radiative heat loss [1,19,20], the burning rate and extinction diameter show much better agreement with experiment.

It is interesting to note from Fig. 6 that radiation loss actually lessens the observed variation in burning rate with time. This result occurs since, early in the droplet lifetime when the diameter is largest, the burning rate is retarded primarily due to radiative heat loss, while later in the droplet lifetime, the burning rate is retarded by the re-vaporization of condensed phase water.

Figure 7 is a plot of the measured and calculated (including radiation) flame position for the experiments shown in Figs 5 and 6. Agreement between experiments and the model are quite remarkable. In each case, the quasi-steady flame position is calculated to within 0.5 normalized diameter of the experimental measurements. The calculated flame position is less sensitive to radiation effects than the burning rate or extinction diameter. For example, for a 5 mm methanol droplet, the quasi-steady flame position decreases by roughly 10% due to radiation loss while the burning rate decreases by 40%.

Comparison of model results with drop tower experiments [17] as well as FSDC-1 results [18] show that because of radiation, the burning rate decreases for increasing initial diameters larger than about 1.5 mm. A similar dependence of burning rate on drop size has been observed in microgravity n-heptane droplet combustion experiments in which soot was produced and soot-shells were observed [24,25]. The results presented here, as well as computations in progress, clearly show that non-luminous radiation can significantly affect the burning rate of n-heptane droplet combustion, even in the absence of sooting.

Figure 8 shows the measured extinction diameter as a function of initial diameter for pure methanol and methanol/water droplets. The experimental results show a nearly linear increase in extinction diameter with increasing initial diameter. By neglecting radiation, a linear increase in extinction diameter with increasing initial diameter has been previously predicted numerically [5] and asymptotically [26] for initially pure methanol droplets. Numerically, this result is only observed if the liquid phase internal motions are assumed significantly enhance liquid phase mass transport.

Thus, the results shown in Fig. 8 suggest the presence of liquid phase motions within the interior of the droplet. Such motions can result from experimental

methods of droplet generation and deployment and they may also be caused by thermal and / or solutal Marangoni effects [5,17,26].

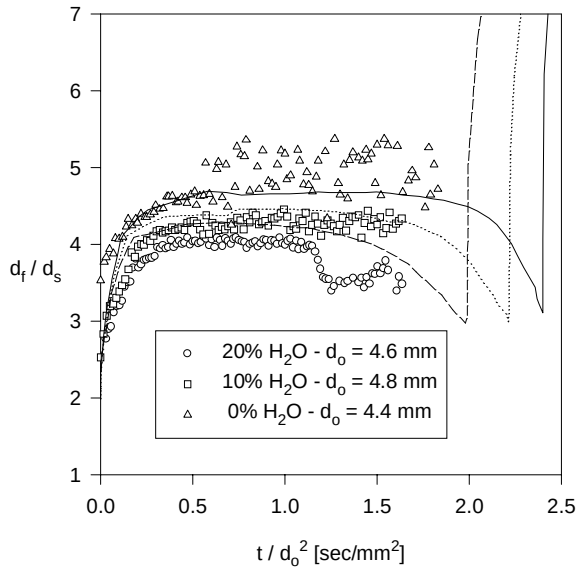

Figure 7. Measured and calculated flame position for 5 mm methanol/water droplets.

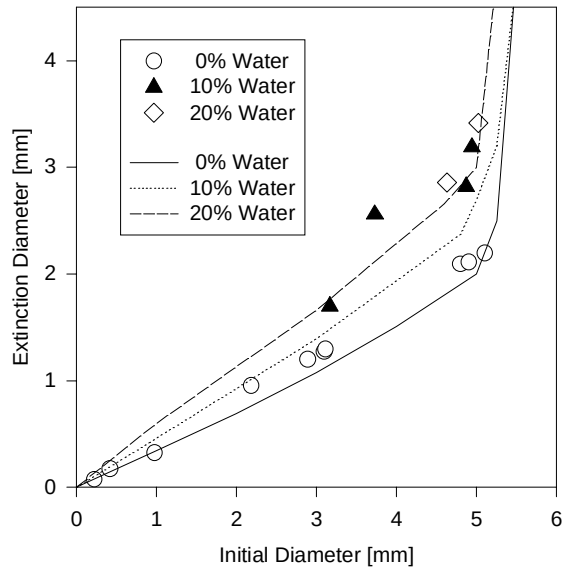

Figure 8. Extinction diameter as a function of initial diameter for methanol/water mixtures. Symbols are experimental results; Lines are calculated results.

The calculations shown in Fig. 8 (which include the effect of radiation) show a nearly linear increase in extinction diameter with increasing initial diameter until a critical initial diameter is reached. For larger initial diameters, the extinction diameter quickly approaches the initial diameter because extinction occurs before the establishment of quasi-steady burning. The radiative extinction phenomena for droplet burning was studied by Chao, *et al* [27] using asymptotics.

In FSDC-1 experiments on methanol and methanol / water mixtures, large droplets were exceedingly difficult to ignite and required several applications of the ignition source. It should be noted, however, that the time-dependent model employed here predicts that droplets larger than the critical diameter noted above, ignite but extinguish after very short, unsteady burning times. Transient burning may exist for varying times dependent on the ignition energy, but quasi steady burning will not occur prior to extinction.

Summary

Here, it has been shown that isolated droplet combustion problems can be utilized to develop, validate, and study the interactions of physical and chemical sub-models for chemically reacting systems. Thus, numerical modeling methodology and sub-model refinements for physical and chemical processes, along with advances in experimental diagnostics, add yet another uni-dimensional combustion venue to those previously available (i.e. gaseous, laminar premixed and diffusion flames). Simultaneous comparison of multiple parameters in such venues give increased confidence in the developed sub-models and their interactions. The resulting complex sub-models yield the bases for developing simplified representations that are compatible with the computational constraints of multi-dimensional models for heterogeneous combustion problems such as sprays.

References

1. Marchese, A. J., Ph. D. Dissertation, Department of M.A.E., Princeton University (1996).

2. Held, T. J., Marchese, A. J., and Dryer, F. L., *Comb. Sci. Tech.*, In press (1996).

3. Cho, S. Y., Yetter, R. A., and Dryer, F. L., *J. Comp. Phys.* **102**, 160-179 (1992).

4. Kee, R. J., Dixon-Lewis, J., Warnatz, J. Coltrin, J. A., and Miller, J. A.,*SAND86-8246* (1986).

5. Marchese, A.J. and Dryer, F.L., *Combust. Flame,* **105**, 104 (1996).

6. Williams, F. A., and Dryer, F. L. *Science Requirements Document for the Droplet Combustion Experiment*, NASA Lewis Research Center, Cleveland, OH (1994).

7. Faeth, G. M., and Olson (1968). *Transactions of the ASME,* 1793 (1968).

8. Warnatz, J. *Twentieth Symposium (International) on Combustion,* The Combustion Institute, Pittsburgh, PA, 1984, p. 845.

9. Hara, H. and Kumagai, S. *Twenty-third Symposium (International) on Combustion*, The Combustion Institute, Pittsburgh, PA, 1990, p. 1605.

10. Yang, J. C., and Avedisian, C. T. *Twenty-second Symposium (International) on Combustion*, The Combustion Institute, Pittsburgh, PA, 1988, p. 2037.

11. Chung, S. H., and Law, C. K. *Combust. Flame*, **64**, 237 (1986).

12. Choi, M. Y., Cho, S. Y., Dryer, F. L., and Haggard, J. B., Jr. *Microgravity Science and Technology*, Springer-Verlag, **IV/2**, 134 (1991).

13. Bui-Pham, M. and Seshadri, K. *Combust. Sci. and Tech.* **79,** 293 (1991).

14. Hamins and Seshadri, *Combust. Flame* **68**, 295 (1987).

15. Marchese, A. J., Dryer, F. L., Nayagam, V., and Colantonio, R. *Twenty-Sixth Symposium (International) on Combustion*, The Combustion Institute, Pittsburgh, PA, 1996, pp. 1219.

16. Gaydon, A. G. (1974). *The Spectroscopy of Flames*, Chapman and Hall, London, p. 196.

17. Marchese, A. J., Dryer, F. L., Colantonio, R., Nayagam, V. (1996). *Twenty-Sixth Symposium (International) on Combustion*, The Combustion Institute, Pittsburgh, PA, 1996, pp. 1209.

18. Dietrich, D. L., Dryer, F. L, Haggard, J. B., Jr., Nayagam, V., Shaw, B. D., and Williams, F. A. *Twenty-Sixth Symposium (International) on Combustion*, The Combustion Institute, Pittsburgh, PA, 1996, pp. 1201.

19. Marchese, A.J. and Dryer, F. L., *Comb. Sci. Tech.* In press (1997).

20. Marchese, A.J. and Dryer, F.L., Fall Technical Meeting, ESS / CI, Hilton Head, SC, December, 1996.

21. Saitoh, T., Yamazaki, K., and Viskanta, R., *Journal of Thermophysics and Heat Transfer*. **7/**1, 94 (1993).

22. Viskanta, R. and Merriam, R. L., *Journal of Heat Transfer*. 90/**2**, 248 (1968).

23. Tien, C. L., *Thermal Radiation Properties of Gases*. Advances in Heat Transfer, Vol. 5., Academic Press, New York, 1968, pp. 115-193.

24. Choi, M. Y., Dryer, F. L., and Haggard, J. B., Jr., *Twenty-Third Symposium (International) on Combustion*, The Combustion Institute, 1990, p. 1611.

25. Jackson, G. and Avedisian, C. T., *AIAA-93-0130* (1993).

26. Zhang, B. L., Card, J., and Williams, F. A., *Combust. Flame* **105**, 267 (1996).

27. Chao, B. H., Law, C. K., and T'ien, J. S., *Twenty-Third Symposium (International) on Combustion*, The Combustion Institute,1990, p. 523.